AMINO ACID-REGULATED ELECTROLYTES FOR RECHARGEABLE ZINC BATTERIES

A Thesis Presented for the

Master of Science

Degree

The University of Tennessee, Knoxville

Paranjothi Murugan

December 2025

ACKNOWLEDGEMENTS

I would like to express my deepest gratitude to Dr. Yingwen Cheng, Department of Chemistry, University of Tennessee, Knoxville, for his unwavering guidance, mentorship, and continuous support throughout my graduate studies. His insights, encouragement, and dedication have been instrumental in shaping both my research skills and academic development. I am also sincerely thankful to my committee members, Dr. Thanh Do and Dr. Brendon McNicholas, for their valuable feedback, constructive discussions, and generous investment of time in reviewing my research. Their expertise and thoughtful comments have improved the quality of this work. I extend my appreciation to all my lab colleagues and collaborators for their encouragement, helpful discussions, and technical assistance. I am especially grateful to Mr. Dhilip Kanna Ashok Kumar for his significant contributions, guidance, and continuous support throughout various stages of my research. His collaboration and insights have been indispensable to the successful completion of this thesis. I would also like to thank my fellow group members — Bomin Li, Bowen An, Emma Lynch, and Nimai Jana — for fostering a collaborative and motivating research environment that made this journey both productive and enjoyable. Finally, I wish to express my heartfelt thanks to my family and friends for their unconditional love, patience, and encouragement. Their unwavering support has been my greatest source of strength throughout this academic journey.

PREFACE

Aqueous zinc batteries (AZBs) offer a safe, low-cost, and environmentally safe pathway for grid-scale energy storage. However, commercialization has been hindered by zinc dendrite growth during cycling, parasitic hydrogen evolution at zinc electrode- especially in acidic or poorly buffered media- and sluggish redox kinetics at sub-zero temperatures. This thesis investigates a 2.0 M $Zn(ClO_4)_2$ electrolyte modified with L-histidine or L-glutamic acid to address these challenges. Compared with sulfate-based systems, perchlorate anions are weakly coordinating, enabling high ionic conductivity and faster Zn^{2+} desolvation, which benefits interfacial kinetics and supports operation below 0 °C. The amino acids further modulate the Zn^{2+} solvation sheath and locally buffer the interface, suppressing side reactions while promoting uniform nucleation and deposition. Collectively, these effects reduce effective water activity, mitigate hydrogen evolution, and stabilize Zn plating/stripping.

Overall, this work demonstrates improved coulombic efficiency, extended cycle life, and robust sub-zero performance in Zn‖α-MnO_2 cells. These outcomes suggest strong potential for deployment in cold climates and renewable storage applications.

ABSTRACT

Aqueous zinc batteries (AZBs) are promising for grid storage due to their safety, low cost, and eco-friendly nature. However, their application is hindered by challenges like zinc dendrite growth, the hydrogen evolution reaction (HER), and poor low-temperature performance. This study systematically investigates a 2.0 molar (M) zinc perchlorate ($Zn(ClO_4)_2$) electrolyte modified with bio-inspired amino acid additives, L-histidine (0.02 M) and L-glutamic acid (0.05 M). Electrochemical analysis shows that these additives modulate the Zn^{2+} solvation structure, suppress HER, and enable highly reversible plating/stripping with coulombic efficiencies at ~98%. In Zn‖α-MnO_2 full cells, histidine provided superior long-term capacity retention (>80 mAh g^{-1} after 100 cycles). Both additives also maintained a coulombic efficiency consistently ~99% at -20 °C. These findings demonstrate that combining chaotropic perchlorate electrolytes with amino acid additives yields high reversibility, cycling stability, and reliable sub-zero operation, highlighting their potential for grid storage and cold-climate applications.

Keywords: Zinc battery, aqueous electrolyte, zinc perchlorate, hydrogen evolution suppression, amino acid additives, L-histidine, L-glutamic acid**,** cyclic voltammetry**.**

LIST OF ABBREVIATIONS

AZB — Aqueous Zinc Battery

ESS — Energy Storage System

EESS — Electrochemical Energy Storage System

LIB — Lithium-ion battery

CE — Coulombic Efficiency

CV — Cyclic Voltammetry

EIS — Electrochemical Impedance Spectroscopy

GA — L-Glutamic Acid

His — L-Histidine

HER — Hydrogen Evolution Reaction

SHE — Standard Hydrogen Electrode

DFT — Density Functional Theory

PTFE — Polytetrafluoroethylene

SCE — Saturated Calomel Electrode

SEM — Scanning Electron Microscopy

TEM — Transmission Electron Microscopy

XRD — X-ray Diffraction

TABLE OF CONTENTS

LIST OF TABLES

LIST OF FIGURES

CHAPTER ONE

INTRODUCTION AND GENERAL INFORMATION

1.1 The global energy transition demands advanced storage solutions

The global transition from fossil fuels to renewable energy sources, such as solar and wind, is a cornerstone of strategies to mitigate climate change [5]. However, the inherent intermittency and fluctuating power output of these sources pose significant challenges to grid stability, reliability, and the balance between supply and demand [6, 7]. To effectively bridge this gap, the deployment of large-scale, efficient, and safe ESS has become indispensable [6]. Among various ESS technologies, EESS, particularly rechargeable batteries, are highly favored due to their scalability, high efficiency, and declining costs. While LIBs currently dominate the market for portable electronics and electric vehicles, concerns regarding the limited global reserves of lithium, high production costs, and severe safety risks associated with flammable organic electrolytes have spurred the search for alternative battery chemistries [1, 2].

1.2 Aqueous zinc batteries represent a safe and sustainable alternative

AZBs have re-emerged as compelling candidates for grid-scale storage, primarily due to their intrinsic safety and economic advantages [2, 3]. The utilization of non-flammable aqueous electrolytes fundamentally eliminates the risk of thermal runaway and fire, a significant drawback of LIBs. Furthermore, zinc metal is abundant, cost-effective (~$2,800/ton), and environmentally benign, offering a sustainable and scalable material platform [8]. The Zn^{2+}/Zn redox couple provides a high theoretical volumetric capacity of 5854 mAh cm^{-3} and a suitable operating potential (-0.76 V vs. SHE) that lies

within the thermodynamic stability window of water, enabling meaningful cell voltages [3, 9]. These attributes collectively position AZBs as a promising technology for stationary storage applications where safety, cost, and longevity are paramount.

1.3 Fundamental challenges of zinc batteries

Despite their considerable promise, the widespread commercialization of AZBs is hampered by several persistent challenges centered on the zinc metal anode.

1.3.1 Dendritic growth leads to safety hazards and efficiency loss

During repeated cycles of plating and stripping, the uneven distribution of current density and ion flux leads to non-uniform zinc deposition. This results in the formation of dendritic or mossy zinc structures [4]. These dendrites irreversibly consume active material, reducing the battery's CE and pose a critical safety hazard. They can grow through the separator, creating an internal short circuit and potentially leading to battery failure [4, 15]. This phenomenon is known as the "tip effect," where the enhanced electric field at a dendrite's tip preferentially attracts Zn^{2+} ions, accelerating further growth of dendrites.

1.3.2 HER consumes efficiency and alters local pH

The operational potential for zinc plating is very close to the reduction potential of water [28], as summarized in Table 1.1. Consequently, the parasitic HER ($2H_2O + 2e^- \rightarrow H_2 + 2OH^-$) readily occurs in competition with the desired Zn deposition [10, 28]. This side reaction consumes electrons, drastically lowering the CE.

Table 1.1. Comparison of zinc and water reduction potentials over varying pH conditions with reference to the SHE.

Reactions	**E° (V vs SHE)**
$Zn^{2+} + 2e^- \rightarrow Zn$	–0.76 V
Water → H_2 (acidic, pH=0)	–0.41 V
Water → H_2 (neutral, pH=7)	–0.83 V
Water → H_2 (alkaline, pH=14)	–1.24 V

More critically, the generation of OH^- ions leads to a sharp increase in the local pH at the electrode surface, facilitating the precipitation of insulating by-products like zinc hydroxide ($Zn(OH)_2$) [10].

1.3.3 Passivation and cathode dissolution cause rapid performance fade

The $Zn(OH)_2$ layer forms a passivating film on the zinc anode, increasing interfacial resistance and hindering ion transport, which leads to voltage polarization and efficiency loss [1]. In unbuffered electrolytes, the zinc metal is also prone to corrosion, resulting in continuous loss of active material and "self-discharge" even during idle storage [2]. These interconnected challenges are summarized in figure 1.1.

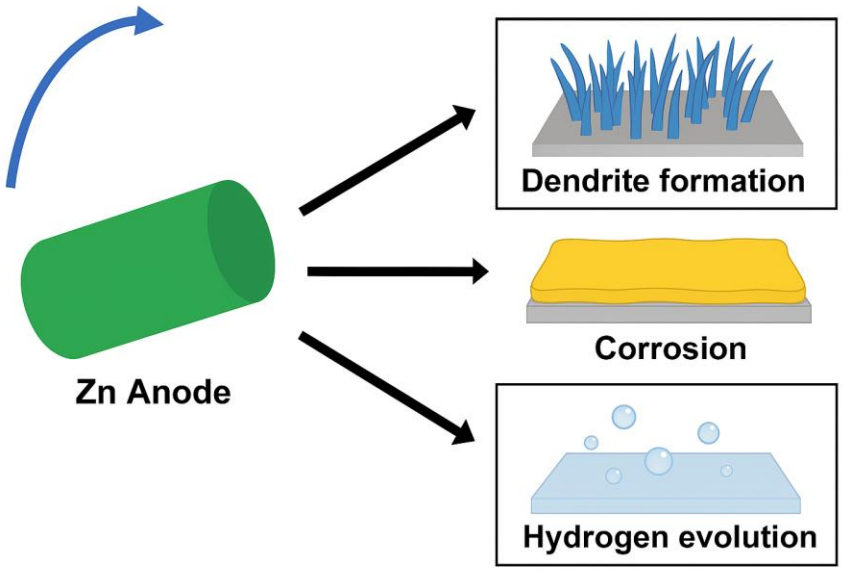

Figure 1.1 Challenges of zinc anode with dendrite formation, corrosion and HER.

1.4 Electrolyte engineering with $Zn(ClO_4)_2$ addresses AZBs challenges

The electrolyte is a central component that governs ion transport, interfacial kinetics, and the suppression of parasitic reactions. Key parameters include the identity and concentration of the zinc salt, the coordinating strength of the anion, and the control of pH [11]. While zinc sulfate ($ZnSO_4$) is widely used, its kosmotropic SO_4^{2-} anion promotes strong ion pairing and the formation of passivating basic zinc salts (e.g., $Zn_4SO_4(OH)_6 \cdot xH_2O$, ZHS), which are detrimental to performance [18]. In this context, $Zn(ClO_4)_2$ presents a compelling alternative. The ClO_4^- anion is chaotropic (disrupts water structure) and weakly coordinating, which facilitates faster Zn^{2+} desolvation kinetics and results in high ionic conductivity (60–65 mS cm^{-1} at 2.0 M) [11, 12]. This property is particularly advantageous for low-temperature operation, as it helps to maintain ion mobility and prevents the formation of rigid ice-like water networks and passivating phases that plague sulfate-based systems. Gao et al. demonstrated that

$Zn(ClO_4)_2$ electrolytes enable Zn‖MnO_2 cells to operate efficiently at temperatures as low as -60 °C [18]. However, a critical limitation of $Zn(ClO_4)_2$ electrolytes is their lack of inherent buffering capacity, which leads to pH drift and exacerbates HER, resulting in poor cycling stability and irreversibility [13]. This underscores the need for innovative stabilization strategies that can function effectively within the unique chaotropic environment of perchlorate electrolytes.

1.5 Amino acid additives offer a bio-inspired path to interface stabilization

A promising approach to stabilize AZB electrolytes is the use of multifunctional additives. Recent research has shifted towards bio-inspired, green molecules, with amino acids standing out as particularly effective candidates. Amino acids possess functional groups that allow them to regulate the Zn^{2+} solvation sheath, adsorb onto electrode surfaces, and buffer local pH changes, as demonstrated in $ZnSO_4$ systems [16, 19, 21, 29]. This precedent establishes a strong foundation for their use; however, their behavior and efficacy in a fundamentally different electrolyte chemistry like $Zn(ClO_4)_2$ remain unexplored.

1.6 A critical research gap exists in amino acid-regulated perchlorate electrolytes

Despite significant advancements, a critical research gap remains. The promising additive strategy of amino acids has been predominantly investigated and developed within $ZnSO_4$-based electrolyte systems [13, 16, 19, 21]. A systematic understanding of their function in the more conductive but less buffered $Zn(ClO_4)_2$ electrolyte is conspicuously absent from the literature. The principal obstacle of pH drift and insufficient buffering in $Zn(ClO_4)_2$ electrolytes creates a unique challenge that amino

acids are uniquely positioned to solve. However, the synergistic effects of coupling chaotropic perchlorate anions with the solvation regulation and interfacial buffering of amino acids have not been thoroughly explored. There is a lack of comparative analysis on how different amino acids with distinct functional groups like the amino group in His versus the carboxylates in GA perform in this specific electrolyte environment. The understanding of their combined impact on long-term cycling stability, interfacial kinetics, and sub-zero temperature performance in full-cell configurations, remains incomplete.

1.7 This thesis aims to develop stable electrolytes for zinc batteries

This thesis work is designed to fill this identified gap by systematically investigating amino acid-regulated $Zn(ClO_4)_2$ electrolytes. The primary objectives are:

- To electrochemically characterize the role of His and GA as additives in a 2.0 M $Zn(ClO_4)_2$ electrolyte.
- To demonstrate enhanced full-cell performance by assembling and testing Zn‖α-MnO_2 batteries.

By achieving these objectives, this research aims to establish a novel, high-performance electrolyte system that combines the intrinsic transport advantages of $Zn(ClO_4)_2$ with the multi-functional stabilization of amino acids, paving the way for more reliable and commercially viable aqueous zinc batteries for cold-climate and grid-scale storage applications.

CHAPTER TWO

LITERATURE REVIEW

2.1 Fundamental electrolyte properties: From conductivity to interfacial transport

The performance of AZBs is governed by bulk electrolyte properties and interfacial phenomena. While high ionic conductivity is desirable, the cation transference number (t_+), representing the fraction of current carried by Zn^{2+}, is more critical for uniform deposition. A low t_+ leads to concentration polarization at the electrode, accelerating dendrite growth. Fundamental studies highlight the advantage of $Zn(ClO_4)_2$. Classic work by Dye et al. measured transference numbers, finding $t_+ = 0.43$ for $Zn(ClO_4)_2$ versus 0.33 for $ZnSO_4$ in 0.1 M solutions [35]. This difference arises from ion pairing: SO_4^{2-} forms mobile anionic complexes like $Zn(SO_4)_2^{2-}$, carrying current away from the anode, while the weakly-coordinating ClO_4^- anion ensures more current is carried by Zn^{2+} cations towards the electrode. This intrinsic property makes $Zn(ClO_4)_2$ superior for maintaining uniform Zn^{2+} flux.

2.2 Engineering the electrode-electrolyte interphase with additives

The performance and longevity of AZBs are fundamentally controlled by the electrode-electrolyte interphase. This dynamic region governs the kinetics of Zn^{2+} ion transport and desolvation. An unstable interphase promotes heterogeneous ion flux, leading to the dendritic zinc growth detailed in the introduction. The strategic use of organic additives is a proven method to engineer a protective interphase. These molecules can adsorb onto the zinc surface, forming a barrier that homogenizes Zn^{2+} flux and

suppresses parasitic side reactions [36]. The mechanism of different additive classes in stabilizing the zinc interphase is summarized in Table 2.1.

Table 2.1. Representative electrolyte additives for zinc anode stabilization and their primary mechanisms.

Additive class	**Example**	**Proposed primary mechanism**	**Ref.**
Small organic molecules	Ethylene glycol	Solvation shell modification, free water reduction	[31]
Ionic liquids	Imidazolium	Adsorption, electric double layer regulation	[32]
Metal cations	In^{3+}	Alloying, reduced nucleation overpotential	[33]
Amino acids	His	Interfacial adsorption, pH buffering	[21]

2.3 Amino acids function as multi-functional interphase regulators

Among the various additive classes, bio-inspired amino acids have garnered significant attention due to their ability to simultaneously modulate multiple aspects of the electrolyte and interphase. Their inherent safety, sustainability, and chemical versatility have made them a popular choice for electrolyte engineering. Different amino acids, with distinct functionalities that influence zinc deposition behavior and overall cell performance. A comparative analysis reveals clear structure-property relationships, as summarized in Table 2.2.

Table 2.2. Performance of various amino acid additives in half-cell (Zn||Zn) configurations using 2.0 M $ZnSO_4$ as a baseline electrolyte.

Amino acid	**Additive concentration**	**Key proposed mechanism**	**Reported CE / performance**	**Ref.**
Glycine	20 mM	Solvation regulation, pH buffering	~98.4% over 600 cycles (1 mA cm^{-2}, 1 mAh cm^{-2})	[36]
Alanine	50 mM	Weak adsorption, solvation shell effect	~99.8% over 4500 cycles (1 mA cm^{-2}, 1 mAh cm^{-2})	[37]
Lysine	10 mM	Strong solvation regulation (dual -NH_2)	~99.8% for 2400 hr (2 mA cm^{-2}, 1 mAh cm^{-2})	[38]
GA	20 mM	Solvation regulation, pH buffering	For 4500 hr (5 mA cm^{-2}, 1.25 mAh cm^{-2})	[19]
His	50 mM	Adsorption, pH buffering	For 4180 hr (2 mA cm^{-2}, 1 mAh cm^{-2})	[21]

Simple amino acids like glycine provide moderate stability through solvation regulation. The enhanced performance of alanine suggests even a small methyl group improves interfacial interaction. More complex structures like lysine are highly effective at low concentrations due to strong, multi-dentate Zn^{2+} coordination. The two primary additives in this thesis exemplify distinct, high-performance pathways: GA acts as a robust solvation regulator, while His functions as an effective interfacial modifier. Both mechanisms enable long-term zinc cycling stability, underscoring the versatility of amino

acids for electrolyte engineering. These molecules act via several mechanisms: adjusting the solvation sheath of Zn^{2+}, adsorbing on the electrode surface, buffering the local pH, and modifying the electric double layer. GA and His possess functional groups (–COOH, $–NH_2$) that are ideal for these regulations. By partially replacing water molecules in the primary solvation shell, they directly reduce free-water activity, which stabilizes nucleation and suppresses the HER [19]. The distinct chemical structures of these amino acids, shown in Figure 2.1 and 2.2.

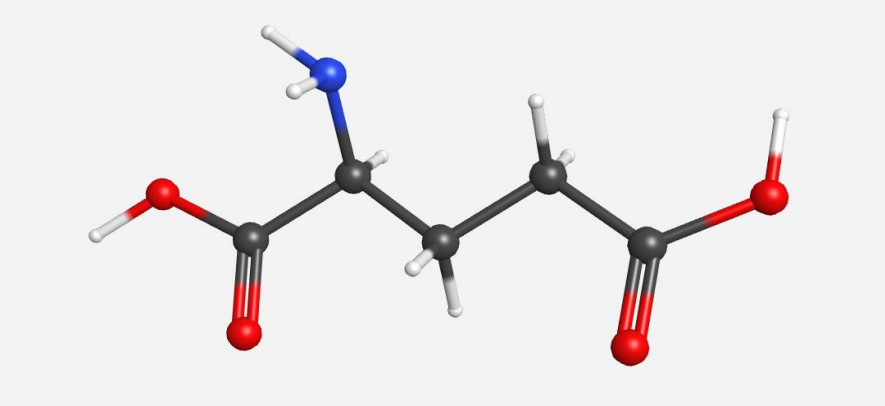

Figure 2.1 Structure of GA (Blue: Nitrogen, Red: Oxygen, Black: Carbon, White: Hydrogen).

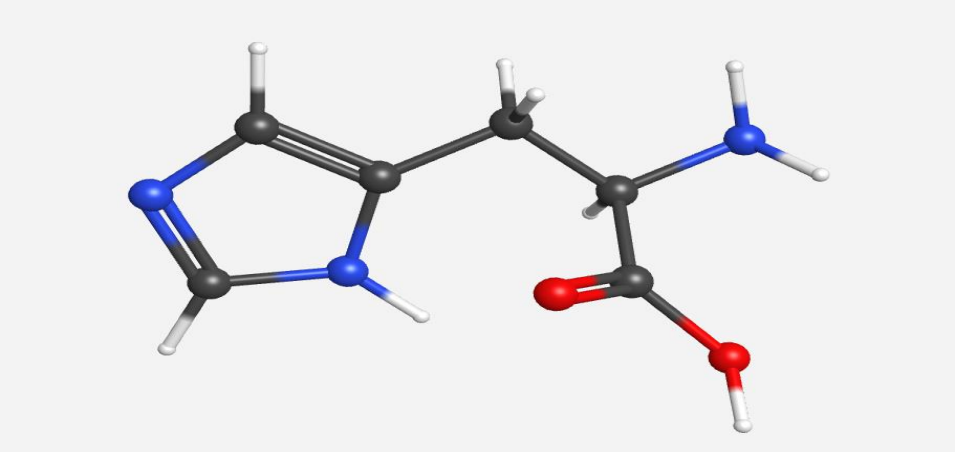

Figure 2.2 Structure of His (Blue: Nitrogen, Red: Oxygen, Black: Carbon, White: Hydrogen).

2.3.1 His: An interfacial modifier

The imidazole and amine functional groups of His enable strong adsorption on Zn (002), as supported by DFT adsorption energy calculations in recent literature [16]. This adsorption modifies surface energetics, steering deposition toward uniform nuclei and denser morphologies. Post-cycling XRD of Zn deposits often show more crystalline with suppressed $Zn(OH)_2$ or ZnO by-products. According to the DFT calculations reported by Dr. Wang et al., the dipole moment of H_2O is 1.99 D, whereas that of His is significantly higher at 5.24 D. This indicates a stronger polar nature and greater ability of His to interact with Zn^{2+} ions compared to water molecules. Furthermore, the HOMO–LUMO energy gap analysis reveals that H_2O possesses an energy level of 7.65 eV, while His exhibits a lower gap of 4.24 eV, suggesting enhanced electronic interaction and higher reactivity toward Zn^{2+}. In addition, the calculated binding energy between Zn and His (-0.60 eV) is notably more negative than that of Zn–H_2O (-0.37 eV), confirming that His can more easily coordinate with Zn^{2+} ions and stabilize the interfacial environment. This

strong adsorption ultimately leads to the formation of fewer, more stable nucleation sites, resulting in uniform and highly reversible Zn plating/stripping [13, 21].

2.3.2 GA: A Solvation Regulator

According to Dr. Zheng et al., DFT calculations demonstrate that the binding energy between Zn and H_2O is -4.47 eV, whereas the Zn–GA interaction is significantly stronger at -7.19 eV. The interaction between GA and H_2O exhibits a comparatively weaker binding energy of -0.52 eV. These results clearly indicate that GA has a stronger affinity for Zn^{2+} ions than water, enabling it to preferentially coordinate with Zn^{2+} and alter the solvation structure in the electrolyte. ^{1}H-NMR analysis further supports this coordination behavior. In a 2.0 M $ZnSO_4$ electrolyte, the water proton resonance appears at 4.768 ppm; upon addition of 50 mM GA, the signal shifts slightly to 4.753 ppm. This downfield shift arises from changes in the local electronic environment of hydrogen atoms as water molecules become partially involved in a new Zn^{2+}–GA–H_2O coordination complex. The observed chemical shift confirms the modification of the hydration shell and the establishment of a new coordination equilibrium between Zn^{2+}, glutamate anions, and water. Raman spectroscopy reveals an O–H stretching band shift from ~3000 cm^{-1} to ~3600 cm^{-1} after the introduction of 50 mM GA signifying reduced free-water activity and a reorganized hydrogen-bonding network. Morphological evidence from SEM images corroborates these findings: Zn deposits formed in plain $ZnSO_4$ electrolytes exhibit a rough, dendritic surface, whereas those obtained with 50 mM GA display a smoother, denser morphology. This confirms that GA effectively

regulates Zn nucleation and growth, mitigating dendrite formation and promoting uniform plating [19].

2.4 The critical role of local pH buffering and her kinetics

The local pH at the electrode-electrolyte interface is a decisive factor in AZB performance, directly influencing HER kinetics and the formation of passivating layers. During plating, the rapid consumption of the few available H^+ ions at the cathode surface creates a localized alkaline environment, even within a bulk acidic electrolyte. This drastic pH swing is a primary driver for the precipitation of insulating $Zn(OH)_2$ and basic zinc salts, which contribute to passivation and capacity fade. Amino acid additives are uniquely suited to mitigate this issue due to their amphoteric nature. They possess both acidic (carboxyl) and basic (amine) functional groups, allowing them to act as efficient molecular buffers within the critical pH window of AZB operation. Their buffering action resists the large pH swings at the interface, thereby stabilizing the electrochemical environment. The effectiveness of specific amino acids is determined by their pK_a values, which dictate their buffering range, as shown in Table 2.3.

Table 2.3. Buffering properties and pH modulation by amino acid additives.

Amino acid	**Relevant pK_a values**	**Effective buffering range**	**ref.**
GA	pK_{a1} (α-COOH) = 2.1, pK_{a2} (γ-COOH) = 4.3	~3.1 - 5.3	[19]
His	pK_a (COOH) = 1.8, pK_a (imidazole) = 6.0	~4.8 - 7.2	[21]

The addition of 50 mM GA to a $ZnSO_4$ electrolyte (pH ≈ 4.2) raises the local pH to ~5.6, situating it perfectly within its buffering range and stabilizing Zn^{2+} coordination [19]. Similarly, His buffers effectively near neutral pH, countering the local alkalization during stripping and suppressing HER [13]. This pH regulation is a vital secondary mechanism that works synergistically with their primary functions of adsorption or solvation regulation to enhance overall cycling reversibility.

CHAPTER THREE

MATERIALS AND METHODS

3.1 Chemicals and reagents

All chemicals were of analytical grade and used without further purification. GA, His, zinc perchlorate hexahydrate ($Zn(ClO_4)_2 \cdot 6H_2O$), and zinc sulfate heptahydrate ($ZnSO_4 \cdot 7H_2O$,) were procured from thermo fisher scientific for electrolyte preparation. Manganese(II) sulfate monohydrate ($MnSO_4 \cdot H_2O$), potassium permanganate ($KMnO_4$), and sulfuric acid (H_2SO_4) from thermo fisher scientific were used for the synthesis of α-MnO_2. Ultra-pure water was used as the solvent for all aqueous solutions**.**

3.2 Electrolyte preparation

The baseline electrolyte, 2.0 M $Zn(ClO_4)_2$, was prepared by dissolving a calculated mass of $Zn(ClO_4)_2 \cdot 6H_2O$ in ultra-pure water under continuous magnetic stirring for 30 minutes at room temperature. Amino acid-modified electrolytes were formulated by dissolving His or GA into the prepared 2.0 M $Zn(ClO_4)_2$ solution to achieve final concentrations of 0.02 M and 0.05 M, respectively. Complete dissolution was ensured by stirring for 60 minutes, with mild heating to 40°C applied intermittently. All electrolytes were stored in sealed polypropylene bottles at ambient temperature to prevent contamination.

3.3 Electrode preparation

Copper foil was cut into 1 cm × 1 cm squares, mechanically polished to remove surface oxides, and subsequently rinsed with ethanol followed by ultra-pure water. The Cu foils were ultrasonicated in ethanol and ultra-pure water for approximately 10 minutes

to ensure thorough surface cleaning. Zinc foil was prepared following a similar polishing and rinsing procedure. A SCE was employed as the reference electrode for all CV measurements.

3.4 α-MnO_2 cathode preparation

The α-MnO_2 cathode active material was synthesized via a hydrothermal method. Briefly, a 0.2 M $MnSO_4$ solution was added dropwise to a vigorously stirred 0.1 M $KMnO_4$ solution. The mixture was transferred to a Teflon-lined autoclave and reacted at 120°C for 12 hours. The resulting precipitate was collected by vacuum filtration, washed thoroughly with ultra-pure water, and dried overnight in a vacuum oven at 80°C. The cathode slurry was formulated by mixing the synthesized α-MnO_2, Super P carbon, and PTFE binder in a 7:2:1 mass ratio. The components were blended into a homogeneous mixture and punched into 12 mm diameter electrodes. The electrodes were dried under vacuum at 100°C for 12 hours prior to cell assembly, yielding an active material mass loading of 3–4 mg per electrode.

3.5 Electrochemical measurements

All measurements were performed on CH instruments CHI601D (serial #A2407) at room temperature (unless otherwise stated) in a three-electrode configuration: Cu working electrode, Zn counter electrode, SCE reference electrode.

3.5.1 CV: Electrochemical analysis:

CV measurements were performed within a potential window of -1.6 V to +0.5 V vs. SCE (unless otherwise stated) at a scan rate of 10 mV s^{-1}. This potential range was chosen to capture Zn plating/stripping.

3.5.2 CE of Zn Plating/Stripping:

The CE of Zn plating/stripping was quantified using a modified protocol in CR2032 coin cells [24]. The cell stack consisted of a Cu working electrode, glass fiber separator (whatman glass fibre), 40 µL of electrolyte, and a Zn foil counter/reference electrode. CE calculated from the final stripping capacity.

3.5.3 Full cell assembly and testing:

Zn‖α-MnO_2 full cells were assembled using the prepared α-MnO_2 cathode, Zn foil anode, glass fiber separator, and 110 µL of electrolyte. Galvanostatic charge-discharge cycling was performed on a Landt CT2001A battery test system within a voltage window of 1.0–1.8 V at 0.33C rate. Low-temperature performance was evaluated at -20 °C**.**

3.6 Optimization of additive concentration

Based on solubility, buffering ranges, and preliminary screening, 0.05 M GA and 0.02 M His were selected. Both 0.05 M GA and 0.02 M His concentrations avoid precipitation in 2.0 M $Zn(ClO_4)_2$.

CHAPTER FOUR

RESULTS AND DISCUSSION

4.1 Additive compatibility: Maintaining core zinc redox activity

CV was employed to evaluate the reversibility, overpotential, and CE of different electrolyte systems and was acquired at 10mV s^{-1} scan rate. All electrolytes showed clear cathodic (plating) and anodic (stripping) peaks, confirming that the fundamental Zn^{2+}/Zn redox reaction remains accessible despite additive presence (Figure 4.1). The baseline 2.0 M $Zn(ClO_4)_2$ electrolyte exhibited a first-cycle CE of approximately 70.4%, indicating significant parasitic reactions. Notably, both amino acid additives substantially improved electrochemical reversibility. The electrolyte containing 0.02 M His additive showed progressively sharper and more symmetric peaks, with CE improving to approximately 99.1%. Similarly, 0.05 M GA additive produced stable, reproducible peak profiles with CE reaching 96.9%, accompanied by reduced background current. These improvements are attributed to suppressed hydrogen evolution through reduced water activity and interfacial stabilization. The overpotential values were extracted from the cathodic peak shifts where 2 M $Zn(ClO_4)_2$ electrolyte, the Zn plating overpotential was approximately 108 mV, indicating higher kinetic resistance for Zn^{2+} reduction. Upon introducing amino acid additives, a significant decrease in overpotential was observed. With His additive, the overpotential decreased to ~60 mV, while GA additive further reduced it to ~38 mV. This reduction in overpotential demonstrates that both additives facilitate more favorable Zn^{2+} nucleation and faster interfacial charge-transfer kinetics.

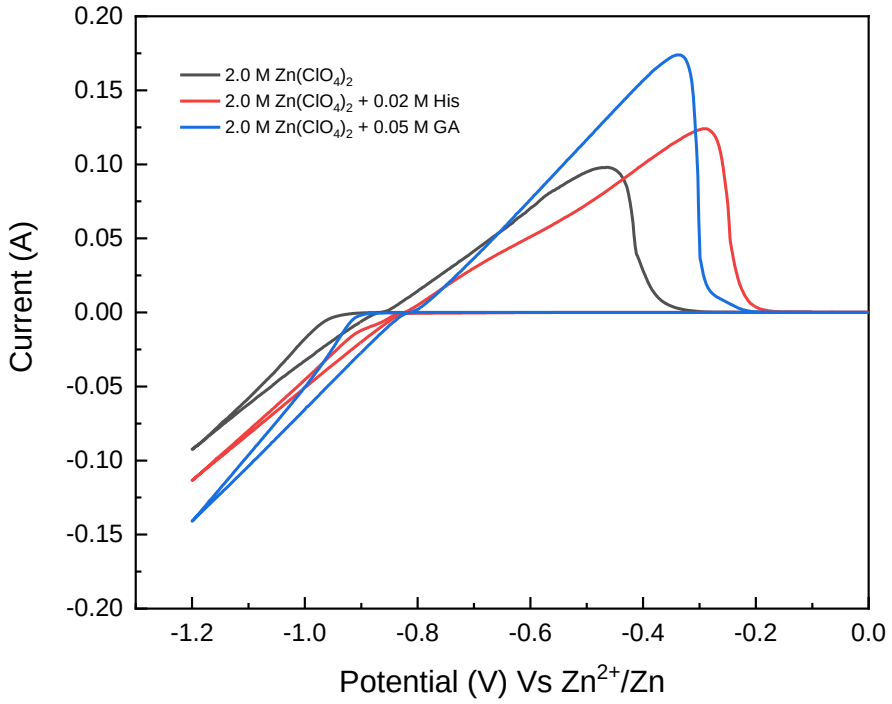

Figure 4.1: Comparison of CV of 2.0 M $Zn(ClO_4)_2$ with and without additives showing Zinc plating/stripping on Cu foil at 10mV s^{-1} scan rate.

4.2 Platting and stripping coin cell studies

The electrochemical plating and stripping studies were conducted by coin cells. CEs were validated with a modified test protocol developed recently to better characterize the efficiency of metal anodes [23]. In this protocol, the current collector was conditioned with one plating step of 6.0 mAh cm^{-2} of metallic Zn. It was stripped completely and electroplated an additional 6.0 mAh cm^{-2} (Qt) Zn. The electrode was cycled 50 times at the current density of 5.0 mA cm^{-2} and capacity of 3.0 mAh cm^{-2} (Qc).

After cycling, the amount of electro-active Zn that remained was quantified by stripping to 0.5 V where the capacity was marked as Qs (Figure 4.2). Using these measured capacities the average faradic efficiency can be calculated by the following equation [28]:

$$|CE| = \frac{(nQc+Qs)}{(nQc+Qt)} \quad (4.1)$$

where n = 50 is the number of cycles, Qc = 3.0 mAh cm^{-2}, Qt = 6.0 mAh cm^{-2}, Qs is active Zn quantified from the final stripping. The voltage profiles was obtained from the three electrolytes using this protocol. 2.0 M $Zn(ClO_4)_2$ has stable cycling and has CE 97.84%, $Zn(ClO_4)_2$ + 0.05 M GA plating plateau is more smooth/clean and the stripping is more coherent. The CE of 0.05 M GA additive is improved to 97.86% with stable cycles. 2.0 M $Zn(ClO_4)_2$ + 0.02 M His has very steady plating and the highest CE = 98.20% (Figure 4.3, 4.4). These data correlates well with CV coulombic efficiency data.

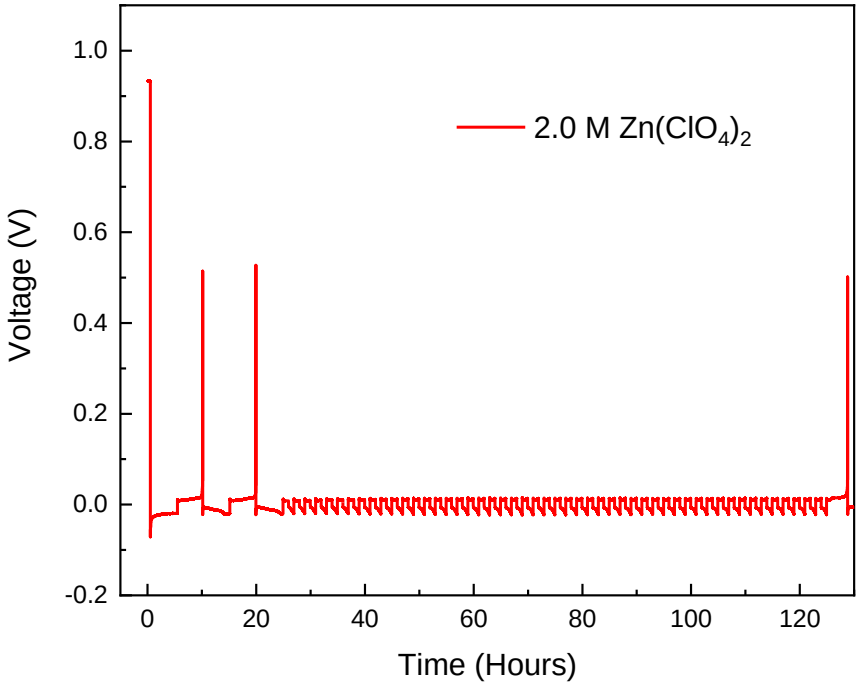

Figure 4.2: Zn plating and striping of 2.0 M $Zn(ClO_4)_2$ electrolyte at 5.0 mA cm^{-2}.

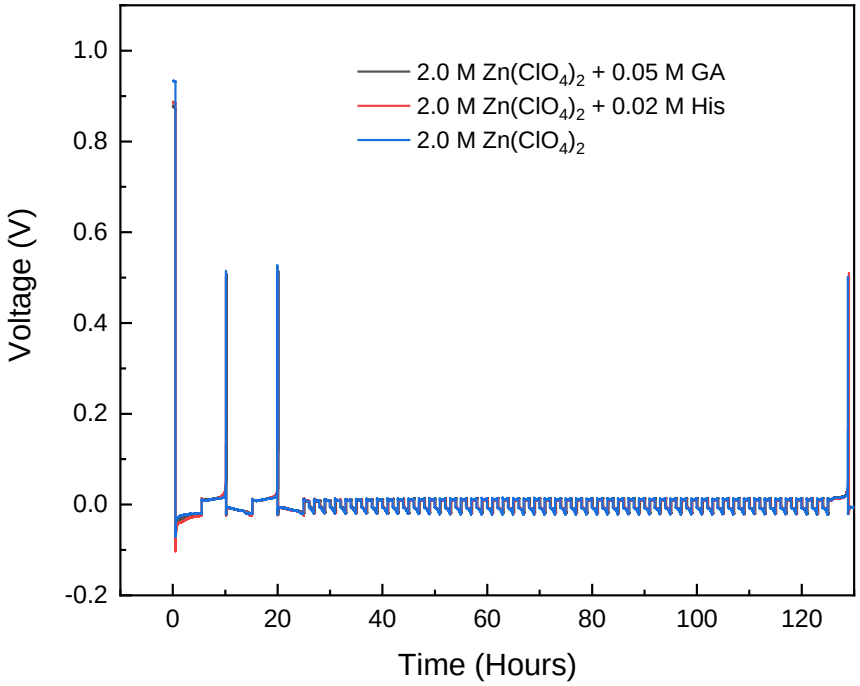

Figure 4.3: Comparison of Zn plating and striping voltage profile for 2.0 M $Zn(ClO_4)_2$ with and without additives at 5.0 mA cm^{-2} .

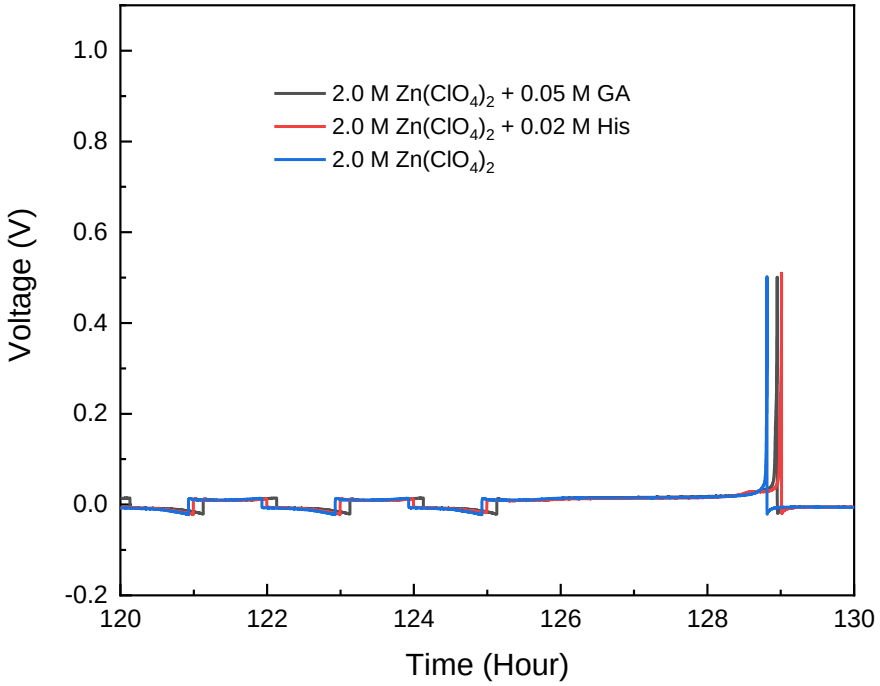

Figure 4.4: Comparison of Zn final striping at 0.5 V for 2.0 M $Zn(ClO_4)_2$ with and without additives at 5.0 mA cm^{-2}.

4.3 Full cell performance evaluation

4.3.1 Room temperature performance:

Zn‖α-MnO_2 full cells were evaluated to assess practical performance implications. At room temperature, the baseline electrolyte showed the highest first-cycle capacity (309.6 mAh g^{-1}) but experienced rapid capacity fade, finishing at only 39.1 mAh g^{-1} after 100 cycles. This rapid degradation is attributed to uncontrolled parasitic reactions, including hydrogen evolution and cathode dissolution exacerbated by free water activity. Both amino acid additives significantly improved capacity retention, though with reduced initial capacity due to modified interfacial kinetics. The GA additive cell showed

moderate stabilization, ending at 57.8 mAh g^{-1} after 100 cycles. His additive cell demonstrated the most substantial improvement, maintaining 80.8 mAh g^{-1} after 100 cycles, representing the best capacity retention among all tested systems (Figure 4.5, 4.6). The first-cycle CE values showed an interesting trend: baseline electrolyte (95.44%) > His additive (89.82%) > GA additive (77.80%). This initial efficiency reduction in additive-containing cells reflects the energy barrier introduced by interfacial modification. However, over 100 cycles, both amino acid systems outperformed the baseline, stabilizing at ~98.5% CE for GA additive, ~98.9% CE for His additive versus 95.44% for baseline, demonstrating their long-term stabilization benefits (Figure 4.6).

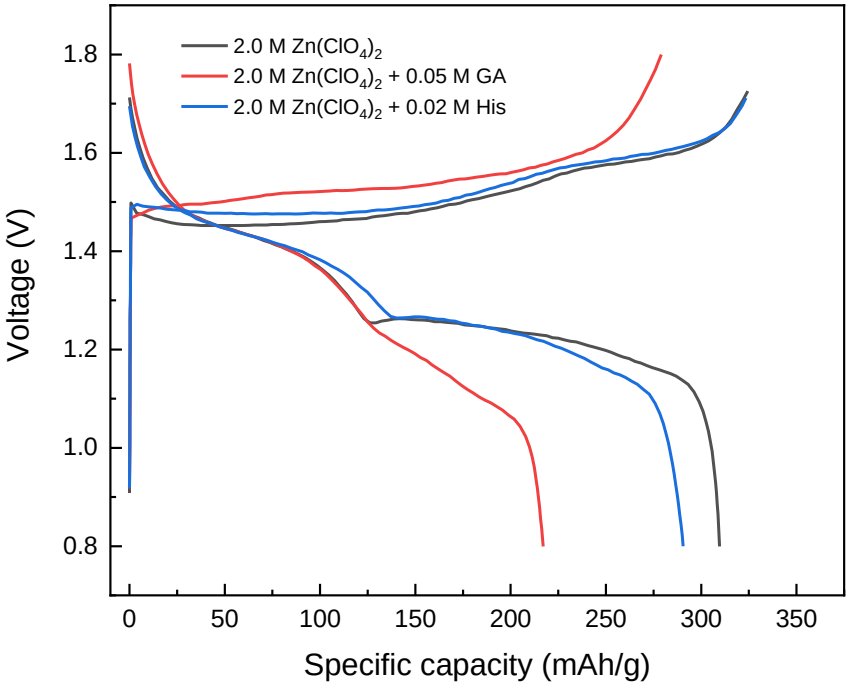

Figure 4.5: Comparison of the voltage profiles from batteries assembled with 2.0 M $Zn(ClO_4)_2$ electrolyte with and without additives, the cycling rate was 0.33 C.

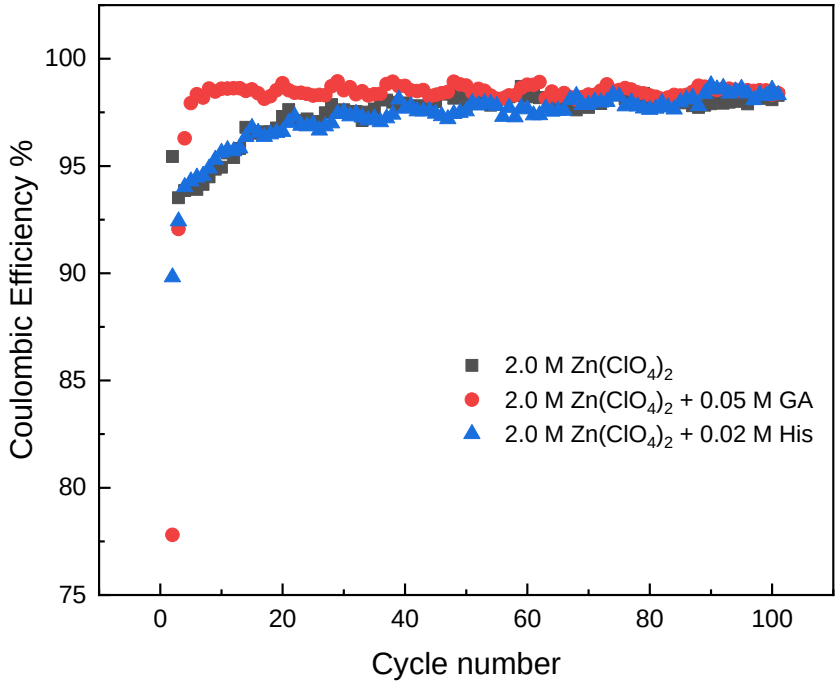

Figure 4.6: Comparison of CE of 2.0 M $Zn(ClO_4)_2$ with and without additives over 100 cycles at room temperature.

4.3.2: Low temperature performance at -20°C

Sub-zero temperature operation revealed particularly striking advantages for the amino acid-modified electrolytes. At -20°C, the baseline electrolyte showed poor performance with initial CE of 74.64% and anomalous behavior including CE spikes exceeding 160%, indicative of incomplete zinc stripping and recovery during discharge. In contrast, both amino acid additives maintained exceptional stability under these challenging conditions. GA and His additives achieved initial CEs of 90.55% and 57.74%, respectively, and rapidly stabilized to near 100% CE for the remaining 100 cycles. The absence of anomalous spikes in additive-containing systems highlights their

effectiveness in maintaining interfacial stability even when bulk electrolyte properties are compromised by low temperature (Figure 4.7). The superior low-temperature performance of amino acid-modified electrolytes can be attributed to their multi-functional nature: solvation sheath modification reduces water activity and freezing point depression, while interfacial buffering maintains stable operation despite reduced ion mobility. These findings demonstrate the particular relevance of amino acid additives for applications requiring operation in cold climates.

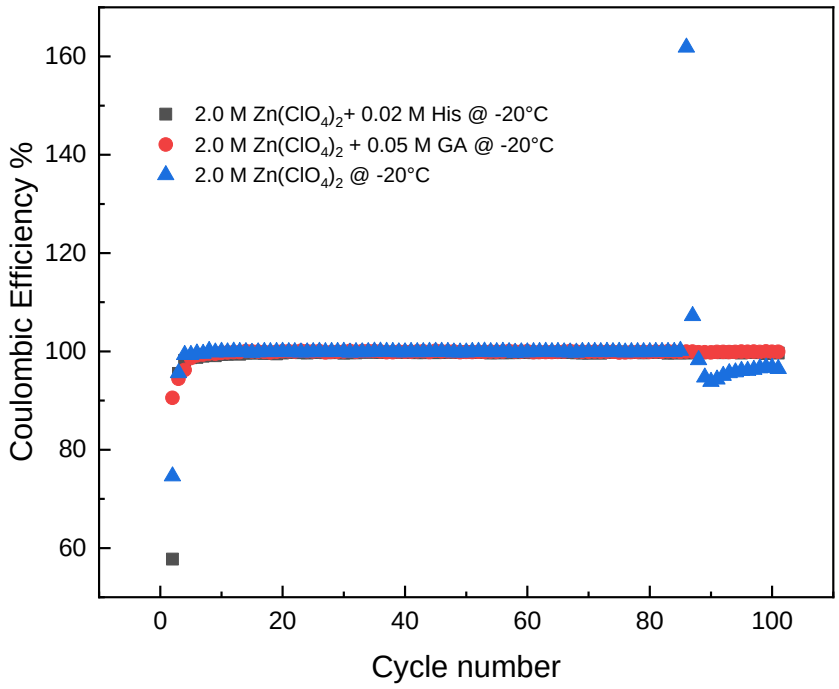

Figure 4.7: Comparison of CE of 2.0 M $Zn(ClO_4)_2$ with and without additives over 100 cycles at -20 °C.

CHAPTER FIVE

CONCLUSIONS AND RECOMMENDATIONS

5.1 Conclusions

This research successfully demonstrates the effectiveness of amino acid additives in stabilizing $Zn(ClO_4)_2$ electrolytes for AZBs. The systematic investigation reveals several key findings: The amino acid additives maintained excellent compatibility with the fundamental zinc redox chemistry while significantly improving electrochemical performance. Both His and GA additives enabled highly reversible zinc plating and stripping, with CE improving from approximately 70.4% in the baseline electrolyte to over 98.9% in modified electrolytes. Full-cell evaluation demonstrated substantial practical benefits. While the baseline electrolyte showed rapid capacity fade, decreasing to 39.1 mAh g^{-1} after 100 cycles, the His additive electrolyte maintained 80.8 mAh g^{-1} under identical conditions. Both amino acid additives demonstrated exceptional stability at low temperatures, maintaining near 100% CE at -20°C compared to the unstable performance of the baseline electrolyte. The multi-functional nature of amino acids, combining interfacial regulation, solvation modification, and pH buffering, addresses multiple failure mechanisms simultaneously. This comprehensive stabilization approach proves particularly valuable under demanding operational conditions, highlighting the potential of bio-inspired molecules for advanced electrolyte engineering.

5.2 Recommendations

Based on the findings of this study, several directions for future research are recommended: Advanced characterization using in-situ and operando techniques such as

XRD, Raman spectroscopy, and SEM would provide direct visualization of additive adsorption dynamics, solvation structure evolution, and interfacial development during cycling. These insights could further elucidate stabilization mechanisms. Systematic optimization of additive chemistry should explore different amino acid combinations, concentrations, and potential synergies with other bio-inspired molecules such as peptides or poly-amino acids. This could lead to enhanced performance through complementary stabilization effects. Cathode stabilization strategies should be integrated with electrolyte optimization. Surface coatings on MnO_2 or additional electrolyte additives that specifically suppress manganese dissolution could address capacity fade mechanisms not fully mitigated by anode-focused approaches. Practical cell validation under realistic conditions is essential. Testing in pouch cell configurations with high areal capacity electrodes (>10 mg cm^{-2}) and limited electrolyte conditions would better demonstrate commercial viability. Scale-up to higher loading cathodes and evaluation under practical cycling protocols would bridge the gap between laboratory research and commercial application.

LIST OF REFERENCES

1. Zhang, N.; Cheng, F.; Liu, J.; Wang, L.; Long, X.; Liu, X.; Chen, J. Rechargeable Aqueous Zinc–Manganese Dioxide Batteries with High Energy and Power Densities. Energy Environ. Sci. 2020, 13, 4625–4635. https://doi.org/10.1039/D1EE02922F.

2. Zhu, K.; Yang, W. Vanadium-Based Cathodes for Aqueous Zinc-Ion Batteries: Mechanisms, Challenges, and Strategies. Accounts of Chemical Research 2024, 57 (19), 2887–2900. https://doi.org/10.1021/acs.accounts.4c00484.

3. Zhang, N.; Chen, X.; Yu, M.; Niu, Z.; Cheng, F.; Chen, J. Materials Chemistry for Rechargeable Zinc-Ion Batteries. Chemical Society Reviews 2020, 49 (13), 4203–4219. https://doi.org/10.1039/c9cs00349e.

4. Zheng, H.; Huang, Y.; Xiao, J.; Zeng, W.; Li, X.; Li, X.; Wang, M.; Lin, Y. Multi-Protection of Zinc Anode via Employing a Natural Additive in Aqueous Zinc Ion Batteries. Chemical Engineering Journal 2023, 468, 143834. https://doi.org/10.1016/j.cej.2023.143834.

5. GER. Global Energy Review 2025; Report No. 20032025, International Energy Agency, Paris, 2025.

6. Energy America. How Weather Affects Solar Panel Output; Energy America Report, 2024. Available online: https://energyamerica.com (accessed March 2025).

7. Santie Oil Company. How Extreme Weather Can Impact Your Wind Turbine; Technical Report, 2024. Available online: https://santieoil.com (accessed March 2025).

8. U.S. Geological Survey. Mineral Commodity Summaries 2024; U.S. Department of the Interior, Washington, DC, 2024.

9. Wei, J.; Zhang, P.; Sun, J.; Liu, Y.; Li, F.; Xu, H.; Ye, R.; Tie, Z.; Sun, L.; Jin, Z. Advanced Electrolytes for High-Performance Aqueous Zinc-Ion Batteries. Chemical Society Reviews 2024. https://doi.org/10.1039/d4cs00584h.

10. Peng, H.; Wang, X.; Yang, F.; Liu, Z.; Lei, H.; Cui, S.; Xie, X.; Ma, G. Regulating Solvation Structure and Inducing Zn (0 0 2) Plane by a Multifunctional Electrolyte Additive toward Dendrite Suppression and Long-Life Zinc Ion Hybrid Capacitors. Chemical Engineering Journal 2023, 474, 145864. https://doi.org/10.1016/j.cej.2023.145864.

11. Cao, J.; Zhang, D.; Zhang, X.; Zeng, Z.; Qin, J.; Huang, Y. Strategies of Regulating Zn2+ Solvation Structures for Dendrite-Free and Side Reaction-Suppressed Zinc-Ion Batteries. Energy & Environmental Science 2022, 15 (2), 499–528. https://doi.org/10.1039/D1EE03377H.

12. Li, Y.; Zhang, Y.; Zhu, Y.; Lai, C.; Wang, Q. Functional Mechanisms and Screening Strategies of Electrolyte Additives for Stable Zinc-Ion Batteries. ACS Applied Energy Materials 2025, 8 (17), 12440–12451. https://doi.org/10.1021/acsaem.5c01155.

13. Di, S.; Nie, X.; Ma, G.; Yuan, W.; Wang, Y.; Liu, Y.; Shen, S.; Zhang, N. Zinc Anode Stabilized by an Organic-Inorganic Hybrid Solid Electrolyte Interphase. Energy storage materials 2021, 43, 375–382. https://doi.org/10.1016/j.ensm.2021.09.021.

14. Parker, J. F.; Chervin, C. N.; Pala, I. R.; Machler, M.; Burz, M. F.; Long, J. W.; Rolison, D. R. Rechargeable Nickel–3D Zinc Batteries: An Energy-Dense, Safer Alternative to Lithium-Ion. Energy Environ. Sci. 2016, 9, 356–361. https://doi.org/10.1039/C6EE01558J.

15. Yi, Z.; Chen, G.; Hou, F.; Wang, L.; Liang, J. Strategies for the Stabilization of Zn Metal Anodes for Zn-Ion Batteries. Advanced Energy Materials 2020, 11 (1), 2003065. https://doi.org/10.1002/aenm.202003065.

16. Peng, M.; Liu, Z.; Hou, M.; Zhang, R.; Cheng, M.; Yu, J.; Feng, Y.; Jiao, P.; Zhang, T.; Zhang, Z.; Xi, C.; Hu, Z.; Zhang, K. An Organic-Inorganic-Integrated Solid Electrolyte Interphase with High-Resilience and Anti-Corrosion for Sustainable Zinc Metal Anode. Angewandte Chemie 2025, 137 (29). https://doi.org/10.1002/ange.202501702.

17. Li, Y.; Fu, J.; Zhong, C.; Wu, T.; Chen, Z.; Hu, W.; Amine, K.; Lu, J. Recent Advances in Flexible Zinc-Based Rechargeable Batteries. Advanced Energy Materials 2018, 9 (1), 1802605. https://doi.org/10.1002/aenm.201802605.

18. Gao, T.; Niu, Z.; Chen, J. High-Energy and Stable Subfreezing Aqueous Zn–MnO_2 Batteries with Selective and Pseudocapacitive Zn-Ion Insertion in MnO_2. Adv. Mater. 2022, 34, 2207122. https://doi.org/10.1002/adma.202207122.

19. Zheng, K.; Zeng, X.; Wang, L.; Chen, L.; Zhang, Y.; Chu, J.; Wang, Y.; Song, J. Multi-Functional Additive with Triple Regulation Mechanisms for Long-Life Zinc-Ion Batteries. ACS Applied Materials & Interfaces 2025, 17 (25), 36728–36738. https://doi.org/10.1021/acsami.5c05730.

20. Zhou, K.; Liu, G.; Zhu, X.; Liu, G.; Yu, X.; Guo, Z.; Wang, Y. Nonflammable Fluorinated Electrolyte Realizing High Voltage Anode-Free Zn Dual-Ion Batteries. Angewandte Chemie International Edition 2024, 64 (1). https://doi.org/10.1002/anie.202413959.

21. Geng, D.; Tang, Y.; Han, X.; Cheng, Z.; Han, L.; Liu, J. Inhibition of Dendrite Growth and Side Reactions Using Histidine as Electrolyte Additive for Aqueous Zn-Ion Batteries. International Journal of Electrochemical Science 2023, 18 (7), 100191. https://doi.org/10.1016/j.ijoes.2023.100191.

22. Zhao, Z.; Li, P.; Zhang, Z.; Zhang, H.; Li, G. Dendrite-Free Zinc Anode Enabled by Buffer-like Additive via Strong Cationic Specific Absorption. Chemical Engineering Journal 2023, 454, 140435. https://doi.org/10.1016/j.cej.2022.140435.

23. Shen, Q.; Wang, Y.; Han, G.; Li, X.; Yuan, T.; Sun, H.; Gong, Y.; Chen, T. Recent Progress in Electrolyte Additives for Highly Reversible Zinc Anodes in Aqueous Zinc Batteries. Batteries 2023, 9 (5), 284–284. https://doi.org/10.3390/batteries9050284.

24. Fayette, M.; Hee Jung Chang; Rodríguez-PérezI. A.; Li, X.; Reed, D. Electrodeposited Zinc-Based Films as Anodes for Aqueous Zinc Batteries. ACS Applied Materials & Interfaces 2020, 12 (38), 42763–42772. https://doi.org/10.1021/acsami.0c10956.

25. Zhang, N. et al. Rechargeable Aqueous Zinc–Manganese Dioxide Batteries with High Energy and Power Densities. Energy Environ. Sci. 2020, 13, 4625–4635.

26. Tribbia, M.; Giorgia Zampardi; Fabio La Mantia. Towards the Commercialization of Rechargeable Aqueous Zinc Ion Batteries: The Challenge of the Zinc Electrodeposition at the Anode. Current opinion in electrochemistry 2023, 38, 101230–101230. https://doi.org/10.1016/j.coelec.2023.101230.

27. Trudgeon, D. P.; Qiu, K.; Li, X.; Mallick, T.; Taiwo, O. O.; Chakrabarti, B.; Yufit, V.; Brandon, N. P.; Crevillen-Garcia, D.; Shah, A. Screening of Effective Electrolyte

Additives for Zinc-Based Redox Flow Battery Systems. Journal of Power Sources 2019, 412, 44–54. https://doi.org/10.1016/j.jpowsour.2018.11.030.

28. Bard, A. J.; Faulkner, L. R. Electrochemical Methods, 2nd ed.; Wiley, 2001.

Wan, F. et al. Aqueous Rechargeable Zinc/Sodium Vanadate Batteries with High Energy and Long Lifetime. Adv. Energy Mater. 2020, 10, 1903179.

29. Ai, Y.; Yang, C.; Yin, Z.; Wang, T.; Gai, T.; Feng, J.; Li, K.; Zhang, W.; Li, Y.; Wang, F.; Chao, D.; Wang, Y.; Zhao, D.; Li, W. Biomimetic Super structured Interphase for Aqueous Zinc-Ion Batteries. Journal of the American Chemical Society 2024, 146 (22), 15496–15505. https://doi.org/10.1021/jacs.4c03943.

30. Zhao, J.; Zhang, X.; Yuan, L.; Han, Z.; Liu, S.; Chu, W.; Yu, H. Interphase Engineering by Electrolyte Additives for Lithium-Rich Layered Oxides: Advances and Perspectives. *ACS Energy Letters* 2021, *6* (7), 2552–2564. https://doi.org/10.1021/acsenergylett.1c00750.

31. Li, X.; Zhou, Y.; Tu, H.; Wang, Z.; Wu, R.; Lu, Y.; Zong, Y.; Liu, Q.; He, J.; Qian, L.; Song, S.; Zhang, Y.; Meng, C.; Yuan, A. Improving Zn Anode Electrochemical Reversibility via Crystallographic Plane Regulation by Polyethylene Glycol Electrolyte Additive. Journal of Solid State Electrochemistry 2024, 28 (9), 3209–3219. https://doi.org/10.1007/s10008-024-05901-x.

32. Solanki, S.; Jha, S.; Sappidi, P.; Gupta, P. K. Anion-Driven Interfacial Engineering and Solvation Structure Modulation of Imidazolium-Based Ionic Liquid Electrolyte Additives for Enhanced Zn Anode Reversibility. Journal of Power Sources 2025, 656, 238019. https://doi.org/10.1016/j.jpowsour.2025.238019.

33. Chang, S.; Fernando, J.; Swati Katiyar; Morell, G.; Wu, X. Trivalent Indium Metal as a High-Capacity, High-Efficiency, Low-Polarization, and Long-Cycling Anode for Aqueous Batteries. Journal of the American Chemical Society 2023. https://doi.org/10.1021/jacs.3c08677.

34. Purser, E. P.; Stokes, R. H. Transference Numbers in Aqueous Solutions of Zinc Sulfate. Journal of the American Chemical Society 1951, 73 (12), 5650–5652. https://doi.org/10.1021/ja01156a045.

35. Dye, J. L.; Faber, M. P.; Karl, D. J. Transference Numbers and Conductances of Multivalent Salts in Aqueous Solution: Zinc Sulfate and Zinc Perchlorate1. Journal of the American Chemical Society 1960, 82 (2), 314–318. https://doi.org/10.1021/ja01487a016.

36. Guo, Z.; Mo, X.; Xu, Y.; Xu, X.; Shi, L.; Wan, H.; Sun, L.; Zhuang, W.; Song, M. Glycine as a Bi-Functional Electrolyte Additive for Favorable Zn Deposition. Journal of Electronic Materials 2024, 53 (11), 6594–6604. https://doi.org/10.1007/s11664-024-11397-y.

37. Feng, Y.; Yuan, Y.; Cai, G.; Wang, B.; Zhang, J.; Xia, Y.; Guo, S. Multifunctional Amphoteric Additive Alanine Enables High-Performance Wide-PH Zn Metal Anodes. Small 2024, 21 (3), e2405144–e2405144. https://doi.org/10.1002/smll.202405144.

38. Yin, J.; Luo, Y.; Li, M.; Wu, M.; Guo, K.; Wen, Z. Electrolyte Additive L-Lysine Stabilizes the Zinc Electrode in Aqueous Zinc Batteries for Long Cycling Performance. ACS Applied Materials & Interfaces 2024, 16 (39), 53242–53251. https://doi.org/10.1021/acsami.4c11404.

VITA

Paranjothi Murugan

Knoxville, TN | paranjothimurugan22@gmail.com | +1 779-910-8894 | LinkedIn: linkedin.com/in/pjothi/

PROFESSIONAL EXPERIENCE

Experimental Intern — Fraunhofer Institute (UMSICHT) | May 2025 – Jul 2025

Battery Material Experimentalist Intern — Nissan North America | Sep 2024 – Apr 2025

Graduate Teaching Assistant — University of Tennessee | Aug 2023 – Dec 2025

Graduate Teaching Assistant — Northern Illinois University | Dec 2022 – Jul 2023

Undergraduate Research Assistant — CSIR-CECRI | Jan 2019 – May 2022

EDUCATION

Master of Science in Chemistry, University of Tennessee, Knoxville, TN | GPA: 3.43 | 2023 – 2025

Bachelor of Technology in Chemical & Electrochemical Engineering, CSIR-CECRI, India | GPA: 3.7 | 2018 – 2022

CERTIFICATIONS & TRAINING

- Battery MBA, Battery Associates (Scholarship Recipient)
- Skill Development Training Program on Energy Materials, CECRI – 2021
- International Workshop on Emerging Materials, Chettinad College – 2021

PUBLICATION: Metallic Cu Surface Enables Reversible Na Metal Anodes and Stabilizes Anode-Free Sodium Metal Batteries, Journal of the Electrochemical Society 2023. DOI: 10.1149/1945-7111/ad0